

# Dynamics of a helium-4 meniscus on a strongly disordered cesium substrate

Alexis Prevost,\* Etienne Rolley, and Claude Guthmann

*Laboratoire de Physique Statistique de L'École Normale Supérieure, associé au CNRS et aux Universités Paris 6 et 7, 24 rue Lhomond, 75231 Paris Cedex 05, France*

(Received 21 June 2001; revised manuscript received 14 September 2001; published 22 January 2002)

We have studied the dynamics of the contact line of a helium-4 meniscus on a strongly disordered cesium substrate. We have used photolithographic techniques to obtain a controlled disorder with a correlation length  $\xi = 9 \mu\text{m}$ . We observe a strong pinning of the contact line on the defects. We have measured the roughness  $W$  of the contact line as a function of its length  $L$  at the depinning threshold; we find that  $W$  scales as  $L^\zeta$ , and is almost independent of the contact angle  $\theta$  of the meniscus for values between  $4^\circ$  and  $12^\circ$ . The roughness exponent is found to be  $\zeta = 0.56 \pm 0.03$ , which is higher than the value of  $1/3$  predicted at equilibrium. We have analyzed the avalanchelike motion of the contact line, and confirmed the above value of  $\zeta$  by measuring the ratio of the size of the step forward to the length of the line involved in a jump. Most theoretical and numerical calculations assume that the motion of the contact line is quasistatic. We show that this assumption is false for our system, which is weakly dissipative. This probably explains why the dynamical behavior of the contact line depends on the contact angle, while the roughness does not. Whether the underdamped motion of the contact line can account for the value of  $\zeta$  is still an open question.

DOI: 10.1103/PhysRevB.65.064517

PACS number(s): 68.08.Bc, 64.60.Ht

## I. INTRODUCTION

The dynamics of a moving elastic boundary in a random medium has been extensively studied over the last decade. Examples of such systems include vortex lattices in type-II superconductors,<sup>1</sup> domain walls in ferromagnets,<sup>2</sup> charge-density waves,<sup>3</sup> and also the motion of the contact line of a liquid droplet on a heterogeneous solid.<sup>4</sup>

From a theoretical point of view, this is a very appealing problem, as the complex physical behavior of most of these dynamical systems can hopefully be captured using a simple phenomenological model which involves only a limited number of ingredients—typically the stiffness of the interface and the pinning energy of the defects. The balance between these two quantities controls the shape of the interface: the defects distort the interface which, on the other hand, minimizes its elastic energy. When the disorder is strong enough, the interface can adopt many different metastable equilibrium configurations: the system is hysteretic. As a consequence, one has to apply a force  $F_{ext}$  per unit length greater than a critical threshold  $F_c$  in order to move the interface at a finite mean velocity  $v$ . Assuming that the motion of the contact line (CL) is quasistatic and neglecting thermal noise, the equation of motion for the CL reads<sup>5</sup>

$$\mu \left( v + \frac{\partial \eta(x,t)}{\partial t} \right) = F_{ext} + f[x, vt + \eta(x,t)] + \mathcal{K}[\eta], \quad (1)$$

where  $\eta(x,t)$  represents the distortion of the interface from its average position  $vt$ ,  $\mu$  is a dissipative coefficient,  $f(x,y)$  is the random force due to the defects, and  $\mathcal{K}[\eta]$  is an elastic restoring force. In many systems, such as a liquid invading a porous medium, the elastic force is short ranged and the elastic interaction is then local.<sup>6</sup>

As first pointed out by Joanny and de Gennes,<sup>7</sup> the stiffness of a CL arises from the liquid-vapor surface tension: the energy associated with a distortion of the CL is mainly due to

the increase of the area of the meniscus. Thus the elastic interaction is long ranged. In the limit of small contact angles  $\theta$ , one finds

$$\mathcal{K}[\eta] = -\frac{1}{\pi} \gamma_{lv} \sin^2 \theta \int dx' \frac{\eta(x',t)}{(x-x')^2}, \quad (2)$$

where the summation is taken over the whole CL;  $\gamma_{lv}$  is the liquid-vapor surface tension.

Heterogeneities of the surface induce local fluctuations of the spreading coefficient  $S \equiv \gamma_{sv} - (\gamma_{sl} + \gamma_{lv})$  ( $\gamma_{sl}$  and  $\gamma_{sv}$  are the solid-liquid and solid-vapor interfacial energies, respectively). The random force  $f$  in Eq. (1) is equal to these fluctuations:  $f(x,y) = S(x,y) - \langle S(x,y) \rangle$ . The amplitude  $\Delta S$  of the disorder can then be characterized using the second moment of  $f(x,y)$ :  $\Delta S^2 \equiv \langle f(x,y)^2 \rangle$ .

Theoretical and numerical studies have been devoted to solve Eq. (1) assuming the elastic force given by expression (2). Close to the depinning threshold  $F_c$ , one expects by analogy to critical phenomena, that the roughness  $W$  of the CL, which characterizes the fluctuations of the CL around its average position, varies with its length  $L$  like  $L^\zeta$  where  $\zeta$  is referred to as the roughness exponent. Functional-renormalization-group (FRG) calculations give  $\zeta = 1/3$  to first order in perturbation theory.<sup>5</sup> This value coincides with the value at equilibrium ( $F_{ext} = 0$ ), which was first obtained by Huse (see Ref. 4) using Imry-Ma arguments, and more recently derived by Hazareesing and Mézard<sup>8</sup> using replica calculations. A previous experiment on a weakly disordered substrate by Rolley *et al.*<sup>9</sup> is in agreement with this prediction, as well as with the scaling of  $W$  for short length scales, i.e., below the Larkin length. Furthermore, the numerical results of Tanguy *et al.*<sup>10</sup> and Zhou and Robbins<sup>11</sup> confirmed that  $\zeta \approx 1/3$  for large length scales.

In this paper, we present experimental results which are obtained on a substrate with strong and well-characterized disorder. We measured the roughness of the CL, and found  $\zeta$

to be greater than  $1/2$ , in contrast with the consensus which seemed to prevail up to now. We have also analyzed the CL dynamics. We found that, when the CL depins from the defects, the local velocity is much higher than the mean velocity  $v$ , so that the usual assumption of a quasistatic motion breaks down. This may be the reason for the unexpected measured value of  $\zeta$ . It is also possible that the one loop FRG calculation is not valid, as suggested by Chauve *et al.*<sup>12</sup>

This paper is organized as follows. In Sec. II, we first describe the experimental setup, as well as the fabrication of the heterogeneous substrate and a description of the image processing. In Sec. III, we qualitatively describe the motion of the CL. In Sec. IV, we then describe the measurements of the roughness of the CL. Finally, we perform an analysis of the CL dynamics in Sec. V. Section VI is devoted to a discussion of our results.

## II. EXPERIMENTAL SETUP

### A. Helium-cesium system

Since a theoretical prediction in 1991 (Ref. 13) and the experimental verification the same year<sup>14</sup> that superfluid helium-4 does not wet cesium below  $T_w \approx 2$  K, the helium-cesium system has proven to be a model system for studying wetting phenomena, such as the prewetting transition<sup>15</sup> and the roughness of the CL,<sup>16</sup> for various reasons. The thermodynamic properties of helium-4 are known with great accuracy. It is the only element to remain liquid at  $T=0$  K, which makes it extremely pure, a property which is harder to meet for ordinary liquids (only its isotope helium-3 can be found in proportions as low as  $10^{-7}$ ). A major advantage of working at low temperatures is that one avoids any contamination of the cesium substrate, and it is possible to work with the exact same substrate repeatedly. The absence of a triple point allows one to vary the temperature over a wide range between 0 and 2 K. By changing the temperature, the contact angle  $\theta$  can be decreased from about  $25^\circ$  at low temperature down to zero at  $T_w$ . Furthermore, helium is superfluid for  $T \leq T_w$ , so that bulk dissipation is extremely low. This has proven to be an adequate property in observing a thermally activated motion of the CL when the length scale of the disorder is mesoscopic.<sup>17</sup>

### B. Fabrication of the disordered cesium surfaces

The disordered substrates are obtained in two steps. First, we use microphotolithography techniques to obtain resin defects randomly distributed over a perfect optical gold mirror (Fig. 1). The gold substrate is coated with a layer of photoresistive resin, Hoechst AZ 5740, at a spin rate of 1500 revolutions per minute. The layer is then exposed to light through a pattern mask, and the exposed resin is washed away through the development process. One is left with one million resin defects deposited over a square  $21 \times 21$  mm<sup>2</sup> surface. The defects have a flat-top shape, and appear rather more roughly cylindrical than cubic as was expected; their lateral size is about  $9 \mu\text{m}$  and their height is  $10 \mu\text{m}$ . Due to the randomness of the deposition process, some defects can merge and form clusters, as shown in Fig. 1.

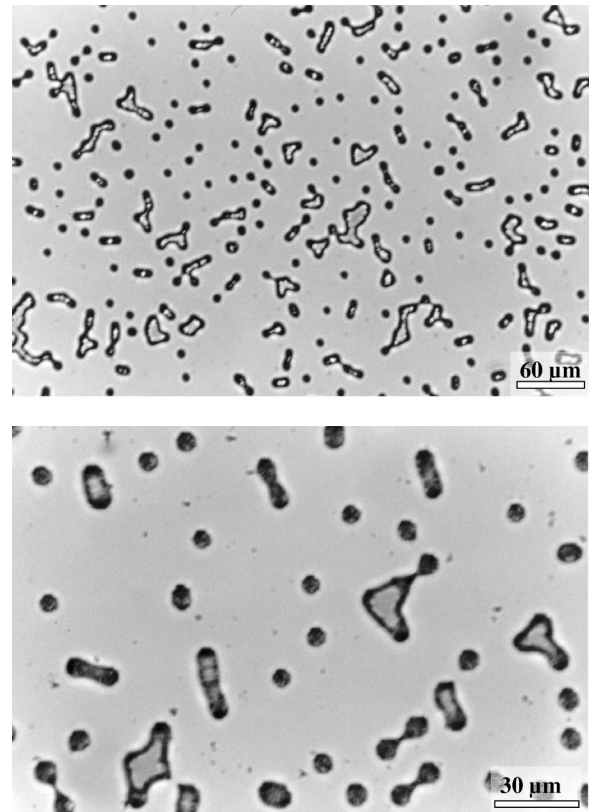


FIG. 1. Pictures of the substrate at two different magnifications. Using microphotolithography techniques, two types of defects were generated: isolated defects which are roughly cylindrical with a nearly flat top, and clusters of defects which result from allowing overlapping.

These clusters have a small effect on the size distribution of the defects, as seen in Fig. 2: the main peak of the distribution which corresponds to the isolated defects is much larger than the second peak, very likely related to the clusters. When plotted in a log-log scale, this distribution shows

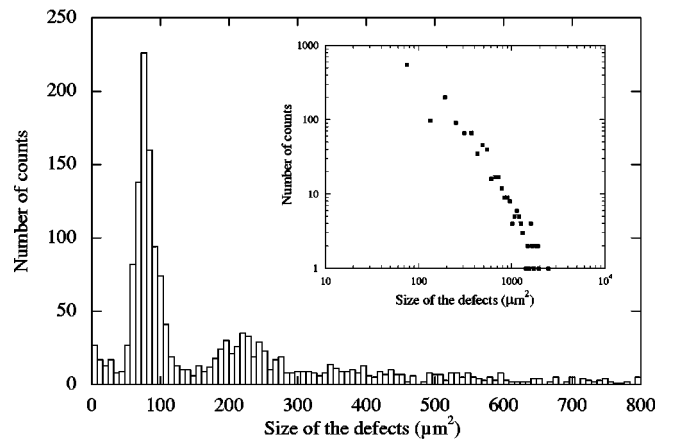


FIG. 2. Size distribution of the defects. The main peak is due to isolated defects of size  $8.7 \pm 0.3 \mu\text{m}$ . A second peak in the distribution can be clearly identified. It corresponds to the existence of clusters, as clearly seen in Fig. 1. Inset: size distribution of the defects on a log-log scale, showing a fast decay.

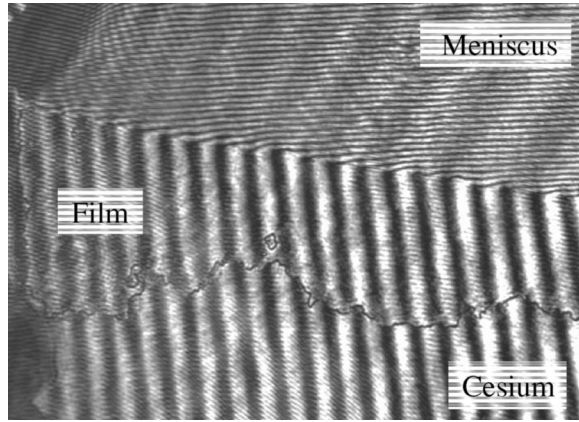


FIG. 3. Equal thickness fringes image of the cell (top view). In the upper part of the picture, the orientation of the fringes is changed by the presence of the meniscus. Ahead of the meniscus, the helium-4 film induces a shift of the fringes pattern as one crosses the film front. This shift was measured to correspond to a film thickness of  $10 \mu\text{m}$ , which is exactly the height of the defects. The CL as well as the edge of the film are distorted by the defects. ( $T=1.6 \text{ K}$ , and the actual image width is  $14 \text{ mm}$ .)

a fast decay. Thus the correlation function of the disorder is short ranged and decays on a length scale  $\xi$  which is of the order of the size of the defects.

In a second step, the substrate with the random defects is placed into a cryostat and a cesium layer is evaporated *in situ* at low temperature, typically  $20 \text{ K}$ . The cesium layer is approximately  $100 \text{ nm}$  thick, so that the topography of the substrate is almost not modified by this additional layer.

### C. Behavior of the helium meniscus on the rough cesium substrate

All the experiments are performed in an optical helium-4 cryostat whose temperature can be regulated within  $1 \text{ mK}$  between  $0.8$  and  $2 \text{ K}$ . The cesium substrate lies on the bottom of the cell and is tilted by a few degrees (the tilt angle  $\alpha$  is typically  $1$  to  $4^\circ$ ) with respect to the horizontal direction, therefore creating a well-defined CL whose average direction is straight. The mean velocity of the CL is controlled by a regulated flow meter in the filling line of the cell in a range from  $0.1$  to  $240 \mu\text{m/s}$ .

The behavior of the helium meniscus on the disordered substrate described previously depends strongly on the temperature of the system. It was reported elsewhere,<sup>18,19</sup> and here we recall briefly how the strong roughness of the substrate modifies the wetting transition. For temperatures below a critical temperature  $T_c$  of about  $1.4 \text{ K}$ , we observe a well-defined meniscus on the dry cesium substrate; the CL, strongly pinned by the defects, is very distorted. Above  $T_c$ , the contact angle is small enough for the liquid to invade by capillarity the channels between the defects, ahead of the meniscus (Fig. 3). The height of the liquid in the channels is equal to the height of the defects. This allows the liquid surface to be flat, as the contact angle at the top edge of the defects is undetermined. Using interferometric measurements (Fig. 3), we confirmed that the thickness of the result-

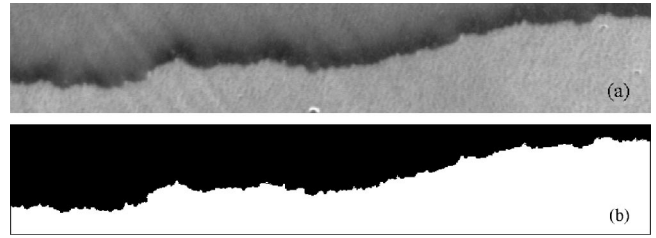


FIG. 4. (a) Raw image of the meniscus which is on top and appears dark, on the binary substrate. (b) Binary image obtained by subtracting from the raw image a reference image with no meniscus present, and by applying a numerical threshold to it. The CL is then defined as the boundary between the black and the white regions ( $\theta=10^\circ$ , and the actual width is  $7 \text{ mm}$ .)

ing film is equal to the height of the defects. The film thickness is homogeneous over the whole sample, and does not depend on temperature. The maximum extension of the film away from the CL, however, does increase with temperature, due to the decrease of the contact angle, and is limited by gravity. It will be larger as  $\alpha$  is lowered. For temperatures above  $1.8 \text{ K}$ , and with  $\alpha=0.7^\circ$ , the liquid completely invades the disordered surface well before the liquid meniscus can be seen (Fig. 3). Unexpectedly, the meniscus does not wet the invaded substrate, although  $85\%$  of the surface is covered with liquid helium with only  $15\%$  with cesium defects (Fig. 4). We took advantage of this unique experimental situation to study the motion of the CL on this disordered substrate, which we call “binary” since the local contact angle has only two possible values:  $\theta_{Cs}$  on the top of the defects, and zero elsewhere. The disorder is completely characterized, and one can ignore the difficulty of properly describing a rough substrate.

The following procedure is used to prepare the binary substrate: helium-4 is condensed in the cell at low temperature (typically  $0.87 \text{ K}$ ) until a liquid meniscus appears. We then cut the flow of helium, and increase the temperature up to  $1.8 \text{ K}$ , favoring invasion and the formation of the film. As its thickness does not depend on the temperature, we can then decrease the temperature to the value at which we wish to perform the experiment. We then turn the flow of helium back on to force the meniscus into motion.

The mean contact angle  $\theta$  of the meniscus on the binary substrate is found to decrease from  $12^\circ$  at low temperature down to zero at the wetting temperature  $T_w=1.95 \text{ K}$ . We have also measured  $\theta_{Cs}$  using flat and homogeneous Cs substrates (see Ref. 18 for a more precise description of the contact angle measurements, which are always done for an advancing meniscus).

### D. Image processing

The meniscus is imaged using white light and various spatial filtering are used to enhance the contrast between the border of the meniscus and the cesium substrate [Fig. 4(a)]. Images of the CL are acquired using a standard CCD camera at a rate of approximately eight frames per second (a rate of  $50 \text{ frames/s}$  can be achieved for short sequences). The images, once acquired, are stored to a hard drive and analyzed

*a posteriori*. To locate the CL, we use the following procedure. First of all, we subtract from the raw image [Fig. 4(a)] an image of the substrate when no meniscus is present in the cell. This has the advantage of removing black pixels due to the disorder along the meniscus, which could be incorrectly considered part of the CL. We then apply a threshold to the resulting difference to obtain a black and white image [Fig. 4(b)]. Additional image processing is then needed, and carefully applied to this image to locate with one pixel accuracy the position of the CL, taken as the black to white boundary. We have checked that the roughness of the CL is independent of the details of the additional image processing. The usual magnification was about  $\times 0.5$ . Higher magnification (up to  $\times 2$ ) was used to check the accuracy of the CL location.

### III. QUALITATIVE DESCRIPTION OF THE CL BEHAVIOR

We used the experimental procedure described in Sec. II to obtain a binary substrate and study the motion of the CL for average contact angles  $\theta$  in the range  $0^\circ$ – $12^\circ$  and for various mean velocities  $v$  ranging from 1 to  $240 \mu\text{m/s}$ . The motion of the line is composed of fast jumps which occur as segments of the CL depin from the defects. This motion resembles an avalanche process. As discussed further below, the velocity of the CL during these jumps is much larger than the mean velocity, so that their detection is very easy.

In a previous study,<sup>17</sup> we showed that the motion of the CL was thermally activated when the length scale of the disorder was mesoscopic, typically for a length scale of the disorder  $\xi$  of about 10 nm. For the binary substrate, the defects are macroscopic in size ( $\xi=9 \mu\text{m}$ ) and the activation energies are consequently very large. Therefore, thermal noise is irrelevant. In this situation, the disorder is said to be quenched: the motion of the CL is entirely deterministic. Indeed, when one does the experiment several times in the same conditions of temperature and flow rate, the visited configurations are always the same. Temperature is then not a relevant parameter in describing the dynamics of the CL. It only acts via the liquid surface tension to change the average contact angle, which therefore is the important quantity to describe the dynamics of the CL on a macroscopic disorder.

Figure 5 shows the successive configurations of the CL at the same contact angle  $\theta=10^\circ$ , for two different helium flow rates. Although there is a difference of two orders of magnitude in the mean velocity of the CL, the pinned configurations remain almost identical. There is almost no effect of the velocity. We could not measure any effect of the velocity on  $\theta$  as well. In other words, the range of mean velocities which are accessible corresponds to forces applied on the CL close to the depinning threshold  $F_c$ .

We have also measured the instantaneous velocity  $v_i$  of the CL during a local jump (i.e., an avalanche). Using an acquisition rate of 50 Hz, we could capture the internal dynamics of an avalanche, as displayed in Fig. 6. We find that  $v_i$  is of the order of 5 mm/s. The value of  $v_i$  is related to the dissipation in the liquid, in the vicinity of the CL. For a classical liquid, the shear flow in the meniscus produces viscous dissipation. For superfluid helium, dissipation is very

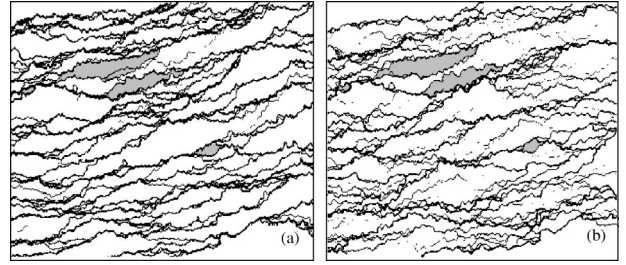


FIG. 5. Images of successive pinned configurations of the CL moving downward. In image (a), the mean velocity  $v$  of the CL is  $1 \mu\text{m/s}$  and images of the meniscus were recorded every 120 ms, whereas on image (b)  $v=240 \mu\text{m/s}$ , with a recording every 20 ms. The shaded regions correspond to a few of the numerous avalanches which are the same on both images. ( $\theta=10^\circ$ , and the actual size of the images is  $6.9 \times 4.9 \text{ mm}^2$ .)

weak, and may arise from the viscosity of the normal component as well as from other mechanisms such as the nucleation of vortex lines.<sup>20</sup>

In order to move away from the vicinity of the depinning threshold  $F_c$ , and to reach the regime where the velocity of the CL is limited by bulk dissipation, it seems reasonable to guess that the mean velocity  $v$  should be of the order of  $v_i$ . Thus one would have to reach mean velocities of the CL at least 20 times larger than the highest value of  $v$  ( $240 \mu\text{m/s}$ ) imposed by our experimental setup. The dynamics of the CL beyond  $F_c$  is thus difficult to study because of the very small bulk dissipation in superfluid helium.

### IV. ROUGHNESS OF THE CONTACT LINE

One way of quantifying the spatial fluctuations or roughness  $W$  of the CL as a function of its length  $L$ , is to measure the following correlation function, defined as the root mean square of the spatial fluctuations of the CL around its average direction:

$$W(L) = \left\{ \overline{[\langle \eta(L+x_0) - \eta(x_0) \rangle]^2} \right\}^{1/2}.$$

The bar denotes an average on  $x_0$  along the line and the brackets an average over successive and independent pinned configurations of the line.



FIG. 6. Close-up look at an avalanche ( $\theta=10^\circ$ ,  $v=240 \mu\text{m/s}$ ). Successive positions of the CL are separated by 20 ms. The black curves are pinned configurations of the CL, defined as configurations where the CL stayed at least for two successive frames. The gray curves are instantaneous, unpinned configurations. (The actual size of the image is  $3.7 \times 1.4 \text{ mm}^2$ .)

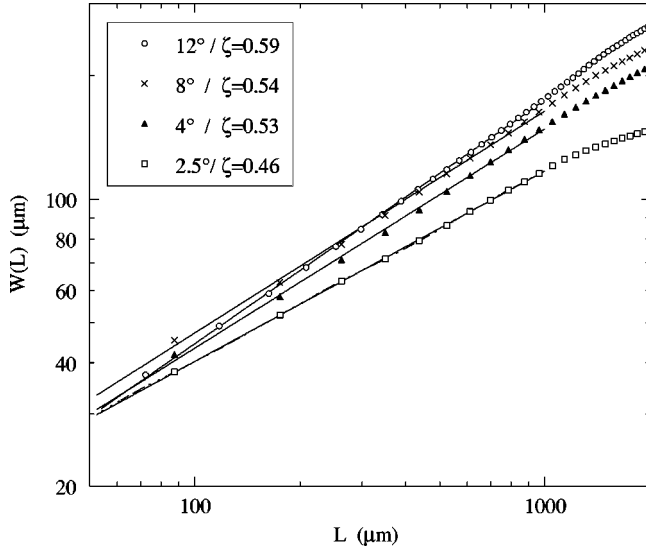


FIG. 7. Roughness  $W$  of the CL for various contact angles. For all contact angles,  $W$  follows a power law of the form  $L^\zeta$ .  $\zeta$  varies slightly, and decreases for contact angles smaller than  $4^\circ$ .

As seen in Fig. 7, the roughness of the CL is almost independent of the contact angle in the range  $4^\circ$ – $12^\circ$ .  $W(L)$  looks slightly steeper for  $\theta=12^\circ$ . This is likely due to a change in the optical setup for this particular run. As the magnification is larger than for the other runs, the pixel discretization is negligible and leads to smaller value of  $W(L)$  for small  $L$ . On the other hand, the small, systematic decrease of  $W(L)$  with  $\theta$  is significant.

In the usual models used to describe the roughness of the CL,<sup>4</sup> the magnitude of  $W$  is controlled by the balance between the stiffness of the line and the strength of the disorder. The stiffness varies like  $\gamma_{lv} \sin^2 \theta$  [see Eq. (2)], and vanishes at the wetting transition. The strength of the disorder  $\Delta S$  can be easily computed for the very special case of a binary substrate. One finds that  $\Delta S$  is equal to  $\gamma_{lv}(1 - \cos \theta_{C_s})$ , so that  $\Delta S$  also vanishes at the transition. Previous measurements of  $\theta$  and  $\theta_{C_s}$  (Ref. 18) are not accurate and reproducible enough to compare the variations of  $\sin^2 \theta$  and  $(1 - \cos \theta_{C_s})$  precisely. Still the values of the contact angles are compatible with a line stiffness vanishing in roughly the same way as the strength of the disorder, leading to distortions of the CL very weakly dependent on  $\theta$ .

When looking for the scaling behavior of  $W(L)$ , one has to determine the cutoff lengths in our experiment. The small one is the correlation length of the disorder  $\xi=9 \mu\text{m}$  and the large one is the effective capillary length  $L_{eff} = (\gamma_{lv}/\rho g \sin \alpha)^{1/2} \approx 4.5 \text{ mm}$ , where  $\rho$  is the liquid density,  $g$  the gravitational acceleration, and  $\alpha$  the tilt angle of the substrate. We find that  $W(L)$  follows roughly a power law for  $L$  ranging between these two cutoff lengths for all values of the contact angle. A more precise value of the roughness exponent  $\zeta$  is obtained by fitting  $W(L)$  by a power law for  $5\xi < L < L_{eff}/5$ ; we find  $\zeta = 0.56 \pm 0.03$  for  $\theta \geq 4^\circ$ . This value has been confirmed first by computing the power spectrum  $\mathcal{H}(q)$  of  $\eta(x)$ , which scales as  $\mathcal{H}(q) \sim q^{-2\zeta}$ , and second by analyzing the aspect ratio of the avalanches as we shall see in the next section.

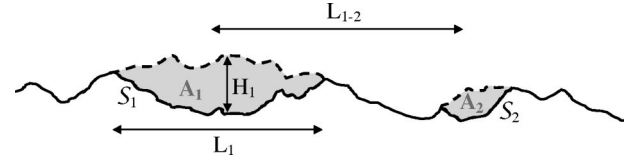


FIG. 8. Definition of the parameters used to characterize an avalanche. Shown by the thick black line is the position of the CL pinned at an instant  $t$ . At an instant  $t + \Delta t$ , two segments  $S_1$  and  $S_2$  of the CL jump simultaneously to dashed line positions. If these two events are separated by a length  $L_{1-2}$  less than the effective capillary length  $L_{eff}$ , we consider them as being part of the same avalanche of size  $A = A_1 + A_2$ , where  $A_1$  and  $A_2$  are the shaded areas swept, respectively, by  $S_1$  and  $S_2$ .

This value of  $\zeta$  is in contradiction with the theoretical predictions at the depinning threshold by Ertas and Kardar,<sup>5</sup> who found  $\zeta = 1/3$  using functional renormalization-group calculations. Numerical estimates are close to the FRG result: Tanguy *et al.* found  $\zeta \approx 0.33$ ,<sup>10</sup> and Zhou *et al.* found  $\zeta \approx 0.39$ .<sup>11</sup> However, Chauve *et al.*<sup>12</sup> extended the one loop calculation of Ertas and Kardar to two loops and found  $\zeta = 0.5 \pm 0.1$ , a value which is tentatively very close to what we find. We will discuss their results in Sec. VI.

## V. DYNAMICS AND SIZE DISTRIBUTION OF THE AVALANCHES

In order to confirm the value we have found for  $\zeta$ , and to shed some light on the dynamics of the CL, we analyze the dynamics of the avalanches. An avalanche occurs whenever a CL which is pinned by the defects jumps to another pinned configuration. We consider that a CL is pinned if its configuration does not change in  $t_{acq} = 120 \text{ ms}$ , the image acquisition period. We have checked that the CL remains locally pinned for a much longer time than  $t_{acq}$ , so there is no risk of lumping together distinct jumps. The only difficulty in detecting avalanches is due to the nonlocal character of the CL elasticity. Let us consider the jump of a local segment  $S_1$  of the CL (Fig. 8). This jump causes a change in the meniscus shape, which can trigger a secondary event for another segment  $S_2$  of the CL. This avalanche can no longer be considered as a segment depinning locally. One must include, as part of the same avalanche, all depinning events which are separated by less than the effective capillary length  $L_{eff}$ . The size  $A$  of the avalanche is then defined as the sum of the individual areas, the height of the avalanche as the maximum of all  $H$ , and its length  $L$  as the total length joining the different segments. *A priori*, identifying disconnected segments as being part of the same avalanche is not so easy, because the corresponding jumps do not occur exactly at the same time. The deformation of the interface propagates at a velocity which is of the order of the velocity  $v_s$  of the surface waves. The surface waves we are interested in are propagating at a distance of the order of the capillary length  $L_c$  behind the CL, where the liquid depth is of the order of  $\theta \times L_c$  [ $L_c = (\gamma_{lv}/\rho g)^{1/2}$ ]. For a wavelength of 1 mm corresponding to a large avalanche, the usual dispersion relation for surface waves in shallow water yields  $v_s \sim 0.1 \text{ m/s}$ , and

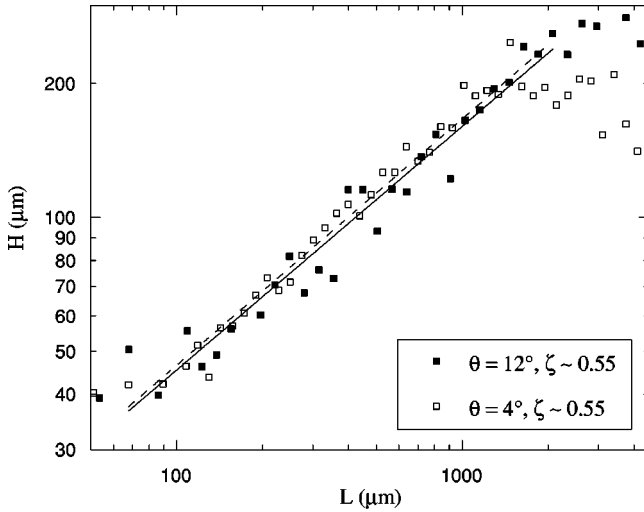


FIG. 9. Height  $H$  of the avalanche jumps as a function of their length  $L$  for two different contact angles ( $12^\circ$  which corresponds to  $T=1.1$  K and  $4^\circ$  and  $T=1.7$  K). The two continuous and dashed lines are power-law fits to the data for  $50 \mu\text{m} < L < 2$  mm. The roughness exponent is found to be  $\zeta \sim 0.55$ , compatible with a more direct analysis.

the maximum delay of secondary events is of the order of  $L_{eff}/v_s \sim 50$  ms. As this delay is smaller than  $t_{acq}$ , we are not able to split primary and secondary events into separate avalanches.

We have first computed the aspect ratio of the avalanches for different contact angles. Figure 9 shows  $H$  as a function of  $L$  for two different angles. One expects that the scaling of  $H(L)$  is the same as the one of the roughness  $W(L)$ . This is the case, and we measure that  $\zeta \approx 0.55$ , confirming the previous measurements.

For forces close to the threshold  $F_c$ , one expects that the distribution in size  $P(A)$  will follow a power law as well, with an exponent  $\gamma_A$ . The distribution  $P(A)$  for two different contact angles is shown in Fig. 10. The power-law de-

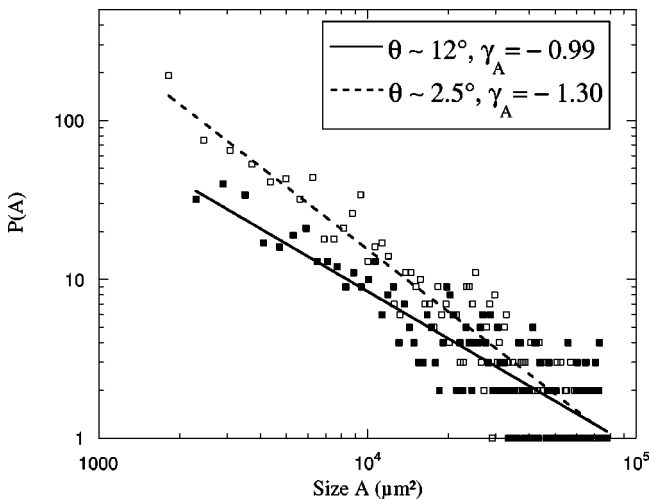


FIG. 10. Log-log plot of the size distribution of the avalanches  $P(A)$  for two different contact angles  $\theta=12^\circ$  and  $2.5^\circ$ . The lines are power law fits to the points:  $P(A) \sim A^{\gamma_A}$ .

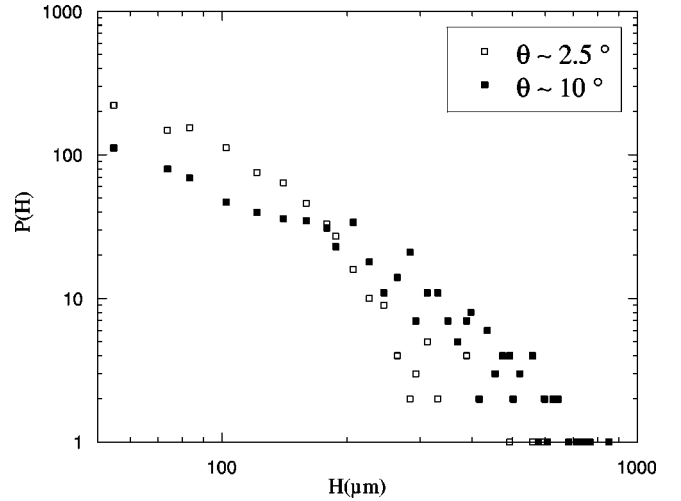


FIG. 11. Log-log plot of the maximum height distribution  $P(H)$  for two different contact angles  $\theta=10^\circ$  and  $2.5^\circ$ .

pendence holds only below a dynamic cutoff length. This cutoff is not relevant in our experiment, since it is presumably larger than  $L_{eff}$ . The dispersion in  $P(A)$  is rather large for large avalanches: the total number of jumps is of the order of a few thousand, and cannot be increased by repeating the experiment because of the deterministic motion of the CL. We have fitted  $P(A)$  with a power law for  $A$  in the range  $1500-15000 \mu\text{m}^2$ . For  $\theta$  larger than  $4^\circ$ , we find  $\gamma_A \approx -1.0$ ; for  $\theta=2.5^\circ$ , we find  $\gamma_A \approx -1.3$ . Numerical simulations of the CL dynamics yielded  $\gamma_A \approx -1.09$ ,<sup>10</sup> and  $\gamma_A = -1.2 \pm 0.1$ .<sup>11</sup> Within uncertainties, the experimental values of  $\gamma_A$  are compatible with the numerical estimates. However these numerical simulations do not provide any explanation for the effect of the contact angle on the distribution  $P(A)$ .

This effect is more clearly seen in Fig. 11, where the distribution in height  $P(H)$  is plotted both for  $\theta=12^\circ$  and  $2.5^\circ$ . At very small contact angles, there is a smaller probability to have large avalanches, and the aspect ratio changes: avalanches appear flatter. This is consistent with what is observed on the roughness  $W$  of the CL.

Interestingly, there is a strong  $\theta$  dependence of the CL dynamics, even in the range  $4^\circ-12^\circ$ , where the roughness  $W$  is almost independent of  $\theta$ . This dependence of the CL dynamics is clearly seen when comparing directly the motion of the CL for different contact angles (Fig. 12). A careful examination of the CL motion shows that the pinned configurations at large  $\theta$  are also pinned configurations at small  $\theta$ . However, going from one of these configurations to the next is done with more intermediate stops when the contact angle  $\theta$  is small. One expects that a line is more easily trapped by the defects if it is soft, that is if the ratio of stiffness to pinning is small. So the occurrence of intermediate stops seems contradictory to the observation that the roughness of the CL is almost independent of  $\theta$ . To summarize, the usual assumption that the dynamics at threshold is entirely controlled by the ratio of stiffness to pinning makes it difficult to understand why the dynamics of the CL is strongly dependent on  $\theta$  while the roughness is not.

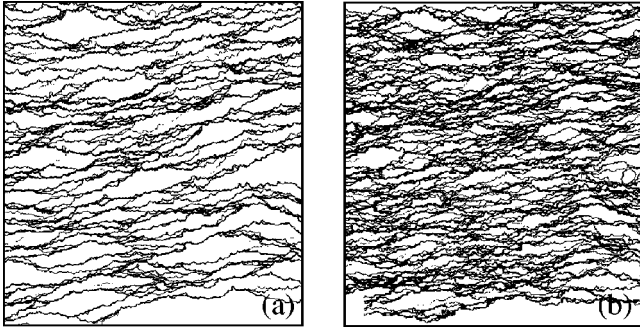


FIG. 12. Dynamics of the CL: effect of the contact angle. On both images, the CL moves downward with the same average velocity  $v = 1 \mu\text{m/s}$ . (a)  $\theta = 12^\circ$ . (b)  $\theta = 4^\circ$ . (The actual size of the images is  $8.1 \times 8.7 \text{ mm}^2$ .)

## VI. DISCUSSION

Our experiments raise two problems. First, the experimental value of the exponent  $\zeta$  ( $0.56 \pm 0.03$ ) is larger than the value  $1/3$  predicted by theories and numerical simulations. Interestingly, the same roughness exponent  $\zeta$  was measured for two-dimensional interfacial rupture fronts propagating at a very small velocity<sup>21</sup> ( $\zeta = 0.55 \pm 0.05$ ). Presumably, this system is very similar to the CL, as described by the same type of nonlocal elastic interaction due to the elastic stresses in the material, and may be weakly dissipative.

Second, it is difficult to reconcile the contact angle dependence of both the roughness and the avalanche size distribution. When decreasing  $\theta$ , the roughness  $W$  slightly decreases which implies that the ratio of pinning to stiffness decreases as well. On the other hand, when decreasing  $\theta$ , more and more pinned configurations appear in the motion of the CL, which rather indicates that the pinning increases.

Let us first discuss the value of  $\zeta$ . The value  $\zeta = 1/3$  was obtained either at equilibrium or using a FRG calculation to one-loop order. However, Chauve *et al.* recently found that extending renormalization-group analysis in dimension  $d = 2 - \epsilon$  beyond one loop leads to a higher  $\zeta$  exponent. They found  $\zeta \approx 0.5$ , which is close to the experimental value. This result is very appealing for our problem. However, one may wonder if the two-loop calculation provides a correct estimate of  $\zeta$ . For lines with a local elasticity, it does: Chauve *et al.*'s estimate of  $\zeta$  is indeed in good agreement with numerical simulations and a recent numerical calculation.<sup>22</sup> However, for a line with a long-range elasticity, the prediction by Chauve *et al.* disagrees with the simulations, which all yield  $\zeta \approx 0.33$ , in the context of both CL (Refs. 10 and 11) and crack propagation.<sup>23,24</sup> A recent numerical calculation gave  $\zeta = 0.390 \pm 0.002$ ,<sup>25</sup> in agreement with Ref. 11. Eventually, let us stress that FRG calculations as well as numerical calculations are based on the same model, given by Eq. (1). So, at threshold, the only parameter which governs the dynamics is still the ratio of pinning to stiffness, and we are left with no explanation for the effect of the contact angle.

Among the hypotheses that lead to Eqs. (1) and (2), the most questionable may be the quasistatic motion of the CL. When one has a closer look at the internal dynamics of an

avalanche (see Fig. 6 for an example), we note that the edge of a depinning area moves laterally with a velocity  $v_{lat} \sim 4 \text{ cm/s}$  for  $\theta = 12^\circ$ . Thus  $v_{lat}$  is of the same order of magnitude as the surface waves velocity  $v_s$  we estimated in Sec. V. The meniscus then cannot adjust its shape adiabatically during an avalanche, and the elastic restoring force is no longer given by Eq. (2), which corresponds to the static force. A phenomenological approach of this situation was recently proposed by Schwarz and Fisher.<sup>26</sup> For weakly dissipative systems such as contact lines or crack fronts in brittle materials, they argued that the motion of a segment of the line causes a transient inertial stress to neighboring segments, in addition to the static elastic stress. When depinning occurs, it may happen that the CL does not stop in the next metastable configuration but to another, further away, because of inertia. Such a mechanism is certainly relevant in our experiment, and can explain why more and more configurations are skipped in the motion of the line when  $\theta$  is increased, as the inertia of the CL increases with the contact angle. Let us also note that Schwarz and Fisher found that the distribution of the sizes of the avalanches changes with the inertia in qualitatively the same way as shown in Fig. 10: the larger the inertia (i.e., the larger  $\theta$ ), the slower the decrease of  $P(A)$ .

We propose the following interpretation to account for what happens when the contact angle is changed. The roughness of the CL changes very little, at least for  $\theta$  in the range  $4^\circ - 12^\circ$ , which means that the properties of the pinned configurations and the balance between the pinning and the stiffness do not change much either. The marked change in the CL dynamics is due to the change of inertia, which is the second parameter controlling the amplitude of the jumps of the CL. Whether inertial effects can also change the nature of the depinning transition is still an open question, as the study by Schwarz and Fisher was restricted to a mean field model.

We wish now to compare the present results with previous ones that we obtained in an earlier experiment, in which the same system (helium on cesium) was used.<sup>9</sup> Let us first recall those previous results. The roughness  $W(L)$  was found to scale as expected from equilibrium calculation,<sup>4,8</sup> that is, with a large scale exponent of order  $1/3$ , and to increase with the temperature. For  $L = 1 \text{ mm}$ , the value of  $W$  increases from  $20 \mu\text{m}$  at  $T = 0.9 \text{ K}$  to  $50 \mu\text{m}$  at  $T = 1.9 \text{ K}$ . So the scaling and the temperature dependence of  $W(L)$  are different from the present results, and the values of  $W$  are significantly smaller.

We think that the main reason for the differences in the two experiments lies in the type of substrate disorder. In an earlier experiment, the disordered substrate was prepared in the same way as now, that is, by evaporation of a Cs layer on a rough surface. However, this rough surface was not obtained by well-controlled photolithographic techniques, but resulted from the oxidation of a first Cs layer whose thickness was smaller than  $0.1 \mu\text{m}$ . This technique led to a roughness whose typical length scale  $\xi$  was about  $20 \mu\text{m}$ , and whose topography was unknown, though presumably less steep than the mesa defects described in the present paper. We argued earlier that the resulting substrate was expected to

present wettable spots, and that it could be described as a binary substrate. However, in light of the present experiment, for which we are sure that the substrate is actually described by a bivalued spreading coefficient  $S$ , we now think that the type of disorder in the two experiments was qualitatively different, as exemplified by the different temperature dependence. The variations of  $S$  with the position on the substrate were presumably much smoother in the earlier experiment, leading to a much weaker pinning of the contact line, and to CL configurations close to the equilibrium ones. This is consistent with the fact that  $W$  was smaller though  $\xi$  was larger by a factor 2.

To summarize, we have studied the properties of the con-

tact line on a strongly disordered substrate. We find a value of the roughness exponent which disagrees with most numerical predictions, and which is in reasonable agreement with the two-loop FRG calculation of Chauve *et al.* However, the underlying assumption that the CL motion is quasistatic is clearly false for our experiment. We think that the CL dynamics is dependent on the fact that the system is weakly dissipative. In particular, the way the CL jumps from one configuration to the next depends on its inertia. To what extent the scaling of the roughness of the CL depends on the inertia is an open question. Studying the wetting of ordinary (viscous) liquids will certainly help to answer the question, and we hope to report on it in the near future.

\*Present address: Georgetown University, Department of Physics, 37th & O streets, Washington DC 20057.

<sup>1</sup>G. Blatter, M. V. Feigel'man, V. B. Geshkenbein, A. I. Larkin, and V. M. Vinokur, *Rev. Mod. Phys.* **66**, 1125 (1994).

<sup>2</sup>K. Dahmen and J. P. Sethna, *Phys. Rev. B* **53**, 14 872 (1996).

<sup>3</sup>O. Narayan and D. S. Fisher, *Phys. Rev. B* **46**, 11 520 (1992).

<sup>4</sup>M. O. Robbins and J. F. Joanny, *Europhys. Lett.* **3**, 729 (1987).

<sup>5</sup>D. Ertas and M. Kardar, *Phys. Rev. E* **49**, 2532 (1994).

<sup>6</sup>A.-L. Barabási and H. E. Stanley, in *Fractal Concepts in Surface Growth* (Cambridge University Press, Cambridge, 1995).

<sup>7</sup>J. F. Joanny and P. G. De Gennes, *J. Chem. Phys.* **81**, 552 (1984).

<sup>8</sup>A. Hazareesing and M. Mézard, *Phys. Rev. E* **60**, 1269 (1999).

<sup>9</sup>E. Rolley, C. Guthmann, R. Gombrowicz, and V. Repain, *Phys. Rev. Lett.* **80**, 2865 (1998).

<sup>10</sup>A. Tanguy, M. Gounelle, and S. Roux, *Phys. Rev. E* **58**, 1577 (1998).

<sup>11</sup>Y. Zhou, Ph.D. thesis, John Hopkins University, Baltimore, 1999; M. O. Robbins (private communication).

<sup>12</sup>P. Chauve, P. Le Doussal, and K. Wiese, *Phys. Rev. Lett.* **86**, 1785 (2001).

<sup>13</sup>E. Cheng, M. W. Cole, W. F. Saam, and J. Treiner, *Phys. Rev. Lett.* **67**, 1007 (1991).

<sup>14</sup>P. J. Nacher and J. Dupont-Roc, *Phys. Rev. Lett.* **67**, 2966 (1991).

<sup>15</sup>J. E. Rutledge and P. Taborek, *Phys. Rev. Lett.* **69**, 937 (1992).

<sup>16</sup>E. Rolley and C. Guthmann, *J. Low Temp. Phys.* **108**, 1 (1997).

<sup>17</sup>A. Prevost, E. Rolley, and C. Guthmann, *Phys. Rev. Lett.* **83**, 348 (1999).

<sup>18</sup>A. Prevost, M. Poujade, E. Rolley, and C. Guthmann, *Physica B* **280**, 80 (2000).

<sup>19</sup>A. Prevost, E. Rolley, C. Guthmann, and M. Poujade, *Physica B* **284-288**, 145 (2000).

<sup>20</sup>J. Wilks, in *Properties of Liquid and Solid Helium* (Oxford University Press, Oxford, 1967).

<sup>21</sup>J. Schmittbuhl and K. J. Måløy, *Phys. Rev. Lett.* **78**, 3888 (1997).

<sup>22</sup>A. Rosso and W. Krauth, *Phys. Rev. Lett.* **87**, 187002 (2001).

<sup>23</sup>J. Schmittbuhl, S. Roux, J.-P. Vilotte, and K. J. Måløy, *Phys. Rev. Lett.* **74**, 1787 (1995).

<sup>24</sup>S. Ramanathan and D. S. Fisher, *Phys. Rev. B* **58**, 6026 (1998).

<sup>25</sup>A. Rosso and W. Krauth, cond-mat/0107527 (unpublished).

<sup>26</sup>J. M. Schwarz and D. S. Fisher, *Phys. Rev. Lett.* **87**, 096107 (2001).